Inorg. Chem. **2002**, *41*, 546–557

Modification of Second-Sphere Communication, Leading to an Unusually High Abundance of the Head-to-Head Conformer of Cisplatin Cross-Link Retro Models

Jamil S. Saad,[†] Tommaso Scarcia,[‡] Kazuo Shinozuka,[§] Giovanni Natile,*[,‡] and Luigi G. Marzilli*[,†]

Department of Chemistry, Emory University, Atlanta, Georgia 30322, Dipartimento Farmaco-Chimico, Università di Bari, Via E. Orabona 4, 70125 Bari, Italy, and Faculty of Engineering, Gunma University, Kiryu City, 376-8515 Gunma, Japan

Received July 16, 2001

Rapid atropisomerization of cisplatin–DNA cross-link models, *cis*-PtA_2**G**$_2$ (A_2 = two amines or a diamine, **G** = guanine derivative, bold font indicating a guanine not linked to another guanine), makes their NMR spectra uninformative. The conformers [two head-to-tail (ΔHT and ΛHT) conformers, one head-to-head (HH) conformer] are detected in (**CCC**)Pt**G**$_2$ retro models (**CCC** = chirality-controlling chelates designed to reduce rotation around the **G** N7 to Pt bond by destabilizing the transition state). Clear trends are found with four **CCC** ligands, 2,2′-bipiperidine (**Bip**) and *N*,*N*′-dimethyl-2,3-diaminobutane (each with *S*,*R*,*R*,*S* and *R*,*S*,*S*,*R* configurations at the chelate ring N, C, C, and N atoms, respectively). *S*,*R*,*R*,*S* ligands favor left-handed **G** base canting and the ΛHT form; *R*,*S*,*S*,*R* ligands favor right-handed canting and the ΔHT form. The HH conformer is normally negligible unless **G** = 5′-GMP. However, understanding this 5′-phosphate effect is complicated by possible interligand interactions of the 5′-phosphate with the N1H of the *cis*-5′-GMP and a **CCC** NH; these interactions are referred to as second-sphere (SSC) and first-to-second-sphere (FSC) communication, respectively. We now investigate the four (**CCC**)-Pt**G**$_2$ models with 1-Me-5′-GMP, a **G** lacking the N1H needed for SSC. The phosphate location makes FSC possible in the major but not the minor HT form. The major form should increase from pH 3 to pH 7 because the phosphate is deprotonated at pH 7. However, the major ΔHT form for the *R*,*S*,*S*,*R* pair did not change in abundance, and the major ΛHT form for the *S*,*R*,*R*,*S* pair actually decreased. Thus, FSC is weak. At pH $\sim$ 7 the HH conformer of the *S*,*R*,*R*,*S* pair had an abundance (40–44%) higher than that in any reported *cis*-PtA_2**G**$_2$ adduct. FSC involving one 1-Me-5′-GMP could play a role. The high HH abundance and use of a pH jump experiment with (*S*,*R*,*R*,*S*)-**Bip**Pt-(1-Me-5′-GMP)$_2$ allowed us to obtain the first deconvoluted CD spectrum for a *cis*-PtA_2**G**$_2$ HH conformer. The CD features for the HH conformer are much weaker than for the HT conformers. Our findings are best interpreted to indicate that FSC is not important in aqueous solution, especially for the HT form. Weak FSC is consistent with recent models of the cross-link in duplexes. In contrast, crystals of fluxional models often reveal FSC, but not the more important SSC. SSC was unrecognized until our retro model studies, and the new results reinforce the value of studying retro models for identifying interactions in solution.

Introduction

Cisplatin (*cis*-Pt$(NH_3)_2Cl_2$) is widely used against a variety of tumors; however, analogues of the type *cis*-PtX_2A_2 [X_2 = anionic leaving ligand(s), A_2 = one diamine or two amine carrier ligands] are generally less active.[1−3] *cis*-PtX_2A_2 compounds target primarily the DNA and bind to the N7 atom of G residues (Figure 1). The most abundant adduct, a 1,2-intrastrand cross-link between adjacent G residues, is thought to be responsible for the anticancer activity.[2−6]

* To whom correspondence should be addressed. E-mail (L.G.M.): lmarzil@emory.edu.
[†] Emory University.
[‡] Università di Bari.
[§] Gunma University.

(1) Sherman, S. E.; Lippard, S. J. *Chem. Rev.* **1987**, *87*, 1153−1181.
(2) Hambley, T. W. *Coord. Chem. Rev.* **1997**, *166*, 181−223.
(3) Jamieson, E. R.; Lippard, S. J. *Chem. Rev.* **1999**, *99*, 2467−2498.
(4) Reedijk, J. *Chem. Commun.* **1996**, 801−806.
(5) Ano, S. O.; Kuklenyik, Z.; Marzilli, L. G. In *Cisplatin: Chemistry and Biochemistry of a Leading Anticancer Drug*; Lippert, B., Ed.; Wiley-VCH: Weinheim, Germany, 1999; pp 247−291.

10.1021/ic010758z CCC: $22.00
Published on Web 01/09/2002

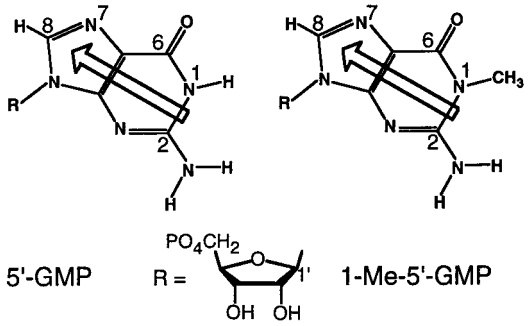

Figure 1. Guanine (left) and 1-methylguanine (right) derivatives (the arrow and its head represent the base and the H8 atom, respectively).

Hydrogen bonding between bound G ligands and the ammines of cisplatin has been an important component of hypotheses concerning the mode of stabilization of distorted DNA induced by drug binding and formation of the intrastrand lesion.[3,7−12] However, examination of an X-ray/NMR-derived model of a duplex 9-oligomer[6] and an X-ray structure of an HMG-bound 16-oligomer,[13] both containing the intrastrand cisplatin lesion, suggests that such hydrogen-bonding interactions involving the Pt−NH_3 groups are at best weak for the 5′-phosphate of the 5′-G in the cross-link and are absent for G O6. Furthermore, if the ammines are replaced by A_2 carrier ligands having sp^3 N atoms bearing two or more alkyl groups, the duplex structures suggest that clashes will result. We hypothesized[6,14] that "The very small size of the NH group, not its hydrogen-bonding ability, is responsible for the good activity exhibited by Pt compounds with amine carrier ligands bearing multiple NH groups."

There is a degree of uncertainty in defining the structure of duplexes bearing Pt drug lesions, and controversy exists as to the details of the structure.[5,6] For this reason and because one might gain better insight into the causes of the distortions and interactions in duplexes by examining small models, many investigators have been drawn to the study of small nonduplex models by both crystallography and spectroscopy. Unfortunately, various problems are encountered with small models also. Crystals of very small molecules usually contain little or no water. In the solid state, H-bonding interactions not present in solution may occur. Also, the charged phosphate groups may be attracted to the cationic Pt center, whereas the electrostatic attraction normally will be less in water. Thus, crystallography may provide misleading or incomplete information about interactions in aqueous solutions. NMR spectroscopy has been used extensively to characterize small synthetic models both with two unlinked residues and with oligonucleotides.[5] We have noted, however, that interpretation of the NMR spectra is complicated by the "dynamic motion problem".[5,15−17] Briefly, when all nuclei of a given species are unique, multiple conformations in fast exchange on the NMR time scale cannot be distinguished from one dominant conformation. One set of resonances is expected for either case, but nuclear Overhauser effect (NOE) cross-peak intensities will be biased toward the conformer with the shortest distance between nuclei. CD spectroscopy does not suffer from dynamic effects, but no CD signatures associated definitively with a particular conformation and useful for determining conformation had been known until recently (see below).

cis-Pt$(NH_3)_2$(d(GpG)), a model of the major adduct formed by cisplatin, has been studied by NMR[5,18,19] and CD spectroscopy.[18] Earlier studies implied that for *cis*-Pt$(NH_3)_2$-(d(GpG)) one conformer is present almost exclusively.[20,21] Partly on the basis of the results for *cis*-$PtA_2\mathbf{G}_2$ complexes ($\mathbf{G}$ = N9-substituted guanine derivative, bold font indicating a guanine not linked to another guanine), we recently postulated that the simplest *cis*-PtA_2(GpG) and *cis*-PtA_2-(dGpG) adducts are highly dynamic mixtures of head-to-head (HH) and head-to-tail (HT) conformers.[17,22]

For *cis*-$PtA_2\mathbf{G}_2$ models, in contrast to oligonucleotide models, an HT form normally dominates, and the less frequently observed HH form is usually a minor form.[15,23−29] *cis*-$PtA_2\mathbf{G}_2$ adducts have two HT atropisomers, designated Δ and Λ (Figure 2), distinguishable by NMR spectroscopy only when the amine ligand(s) or the $\mathbf{G}$ ligands contain a chiral element. *cis*-Pt$(NH_3)_2\mathbf{G}_2$ adducts with $\mathbf{G}$ ligands having chiral sugars could exhibit up to four sets of resonances, one for each C_2-symmetric HT conformer and two for the HH

(6) Marzilli, L. G.; Saad, J. S.; Kuklenyik, Z.; Keating, K. A.; Xu, Y. *J. Am. Chem. Soc.* **2001**, *123*, 2764−2770.
(7) van Garderen, C. J.; Bloemink, M. J.; Richardson, E.; Reedijk, J. *J. Inorg. Biochem.* **1991**, *42*, 199−205.
(8) Reedijk, J. *Inorg. Chim. Acta* **1992**, *198*−*200*, 873−881.
(9) Sherman, S. E.; Gibson, D.; Wang, A.; Lippard, S. J. *J. Am. Chem. Soc.* **1988**, *110*, 7368−7381.
(10) Farrell, N. In *Metal Ions in Biological Systems*; Sigel, A., Sigel, H., Ed.; Marcel Dekker: New York, 1996; Vol. 32, pp 603−639.
(11) Laoui, A.; Kozelka, J.; Chottard, J.-C. *Inorg. Chem.* **1988**, *27*, 2751−2753.
(12) Bloemink, M. J.; Heetebrij, R. J.; Inagaki, K.; Kidani, Y.; Reedijk, J. *Inorg. Chem.* **1992**, *31*, 4656−4661.
(13) Ohndorf, U.-M.; Rould, M. A.; He, Q.; Pabo, C. O.; Lippard, S. J. *Nature* **1999**, *399*, 708−712.
(14) Sullivan, S. T.; Ciccarese, A.; Fanizzi, F. P.; Marzilli, L. G. *J. Am. Chem. Soc.* **2001**, *123*, 9345−9355.
(15) Ano, S. O.; Intini, F. P.; Natile, G.; Marzilli, L. G. *Inorg. Chem.* **1999**, *38*, 2989−2999.
(16) Marzilli, L. G.; Ano, S. O.; Intini, F. P.; Natile, G. *J. Am. Chem. Soc.* **1999**, *121*, 9133−9142.
(17) Williams, K. M.; Cerasino, L.; Natile, G.; Marzilli, L. G. *J. Am. Chem. Soc.* **2000**, *122*, 8021−8030.
(18) Girault, J.-P.; Chottard, G.; Lallemand, J.-Y.; Chottard, J.-C. *Biochemistry* **1982**, *21*, 1352−1356.
(19) den Hartog, J. H. J.; Altona, C.; Chottard, J.-C.; Girault, J.-P.; Lallemand, J.-Y.; de Leeuw, F. A. A. M.; Marcelis, A. T. M.; Reedijk, J. *Nucleic Acids Res.* **1982**, *10*, 4715−4730.
(20) Bloemink, M. J.; Reedijk, J. In *Metal Ions in Biological Systems*; Sigel, H., Sigel, A., Ed.; Marcel Dekker: New York, 1996; Vol. 32, pp 641−685.
(21) Neumann, J.-M.; Tran-Dinh, S.; Girault, J.-P.; Chottard, J.-C.; Huynh-Dinh, T. *Eur. J. Biochem.* **1984**, *141*, 465-472.
(22) Williams, K. M.; Cerasino, L.; Natile, G.; Marzilli, L. G. Unpublished work.
(23) Cramer, R. E.; Dahlstrom, P. L. *J. Am. Chem. Soc.* **1979**, *101*, 3679−3681.
(24) Xu, Y.; Natile, G.; Intini, F. P.; Marzilli, L. G. *J. Am. Chem. Soc.* **1990**, *112*, 8177−8179.
(25) Kiser, D.; Intini, F. P.; Xu, Y. H.; Natile, G.; Marzilli, L. G. *Inorg. Chem.* **1994**, *33*, 4149−4158.
(26) Ano, S. O.; Intini, F. P.; Natile, G.; Marzilli, L. G. *J. Am. Chem. Soc.* **1997**, *119*, 8570−8571.
(27) Marzilli, L. G.; Intini, F. P.; Kiser, D.; Wong, H. C.; Ano, S. O.; Marzilli, P. A.; Natile, G. *Inorg. Chem.* **1998**, *37*, 6898−6905.
(28) Wong, H. C.; Coogan, R.; Intini, F. P.; Natile, G.; Marzilli, L. G. *Inorg. Chem.* **1999**, *38*, 777−787.
(29) Wong, H. C.; Intini, F. P.; Natile, G.; Marzilli, L. G. *Inorg. Chem.* **1999**, *38*, 1006−1014.

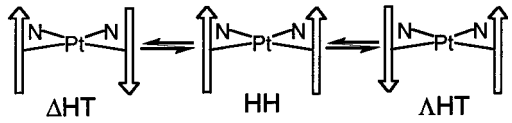

Figure 2. Shorthand representation of ΛHT, ΔHT, and HH conformations with the carrier ligand to the rear. Arrows represent the **G** bases with **G** H8 near the tip and **G** O6 near the blunt end.

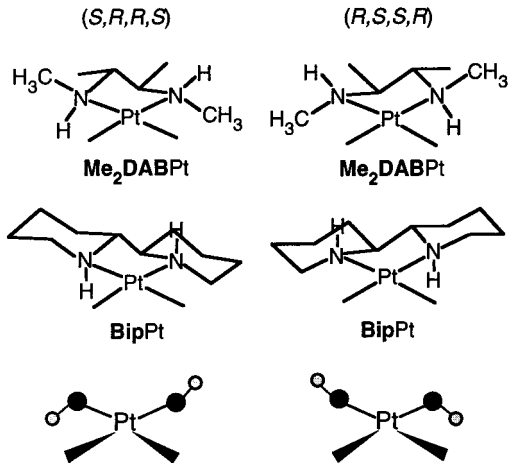

Figure 3. Sketches of the **Bip**Pt and **Me$_2$DAB**Pt moieties with the *S*,*R*,*R*,*S* chiralities on the left and the *R*,*S*,*S*,*R* chiralities on the right. Nitrogen atoms are heavily shaded, while hydrogen atoms are lightly shaded.

conformer; however, these give only one set of NMR resonances.[23,30] This result has long been attributed to the existence of several conformers in fast chemical exchange.[23] This hypothesis is strongly supported by observations that bulky amine ligands can slow rotation of the **G** bases sufficiently to allow detection of different rotamers by NMR spectroscopy.[23−25]

Because complications exist for both linked and unlinked models, we have been developing methods to define spectral parameters (e.g., NMR shifts, CD signal shape) that allow us to assess the nature of the conformers in solution. We have been constructing analogues of cisplatin with carrier ligands designed to reduce the dynamic motion by destabilizing the transition state for Pt−N7 rotation but having bulk in or near the coordination plane, thereby allowing the coexistence of multiple conformers. We have introduced the term "retro modeling" [15] to emphasize that the models we are constructing are more complicated than cisplatin.

We have been utilizing primarily two related retro-model carrier ligands, **Me$_2$DAB** (*N*,*N*′-dimethyl-2,3-diaminobutane) and **Bip** (2,2′-bipiperidine) (Figure 3).[15,24−27] The **Me$_2$DAB**Pt and **Bip**Pt moieties have *S*,*R*,*R*,*S* and *R*,*S*,*S*,*R* C_2-symmetric enantiomeric configurations, where the chiral centers point to the N, C, C, and N chelate ring atoms, respectively (Figure 3). Because the other substituents on the N control the positioning of the NH groups and the chirality of the dominant HT conformers, we call these ligands chirality-controlling chelate (**CCC**) ligands. The major conformer for (**CCC**)-Pt**G**$_2$ adducts is the HT form having the carrier ligand NH located on the opposite side of the **G** O6. The favored form cannot participate in a **G** O6 hydrogen bond, originating the hypothesis that carrier ligand H-bonding is not important.

For *cis*-PtA$_2$**G**$_2$-type adducts, the dominance of HT conformers over the HH form can be attributed to the better dipole (base)−dipole (base) alignment and the lower base−base steric clashes of the HT orientation vs HH orientation. In addition, the favored HT form in (**CCC**)Pt**G**$_2$ retro models with **G** = 5′-GMP can possibly be stabilized by phosphate carrier ligand NH hydrogen bonding; we call this "first-to-second-sphere communication" (FSC). We found that the **G** N1H is a key feature stabilizing the favored HT conformer by participating in hydrogen bonding to the phosphate group of the *cis*-**G**; we call such interligand phosphate−*cis*-**G** N1H interactions "second-sphere communication" (SSC).[31] These findings and the fact that the group most likely to participate in H-bonding in the HH DNA adduct is the 5′-phosphate group[6,9,13] reveal the need to assess FSC, particularly in HH forms of models.

Characterization of the spectral and structural features of the HH conformer is difficult because of its low abundance. The nucleotide 1-Me-5′-GMP (Figure 1) has no N1 proton; hence, SSC cannot favor an HT form.[15,27,31,32] **Me$_2$ppz**Pt(1-Me-5′-GMP)$_2$ (**Me$_2$ppz** = *N*,*N*′-dimethylpiperazine) was 34% HH conformer, a large amount. **Me$_2$ppz** is not chiral and lacks NH groups.[33,34] The absence of NH groups in the **Me$_2$ppz** ligand eliminates the possibility of hydrogen-bonding interactions with the **G** O6 atom/phosphate group. However, there is no way to assess FSC in the 1-Me-5′-GMP adduct. Therefore, we have investigated the four (*S*,*R*,*R*,*S*)- and (*R*,*S*,*S*,*R*)-(**CCC**)Pt(1-Me-5′-GMP)$_2$ adducts. Our investigation provides clear assessments of the role of FSC. We found high amounts of the HH form, making it possible to learn more about this important form than in previous studies. For example, by applying a pH jump cycle, we were able to define better the CD spectral characteristics of the HH conformer.

Experimental Section

Materials. Syntheses of compounds of the form (*S*,*R*,*R*,*S*)-**Me$_2$DAB**Pt(SO$_4$)(H$_2$O), (*R*,*S*,*S*,*R*)-**Me$_2$DAB**Pt(SO$_4$)(H$_2$O), (*S*,*R*,*R*,*S*)-**Bip**Pt(NO$_3$)$_2$, and (*R*,*S*,*S*,*R*)-**Bip**Pt(NO$_3$)$_2$ have been described elsewhere.[24,26] 1-Me-5′-GMP was prepared as described previously.[31]

Methods. A typical preparation involved treatment of ∼2 equiv of 1-Me-5′-GMP with 1 equiv (∼10 mM) of **Me$_2$DAB**Pt(SO$_4$)(H$_2$O) or **Bip**Pt(NO$_3$)$_2$ in D$_2$O (0.6 mL) at pH ∼ 3 and 5 °C. Reactions were monitored by ^{1}H NMR spectroscopy until either no free 1-Me-5′-GMP H8 signal or no change in the H8 signal intensity was observed. Standard DNO$_3$ and NaOD solutions (in D$_2$O) were used for adjusting the pH (uncorrected) of the samples directly in the NMR tubes when necessary.

1D ^{1}H NMR spectra, obtained on a GE GN-Omega 600 or Unity 600 spectrometer, were referenced to the residual HOD peak. In a

(30) Dijt, F. J.; Canters, G. W.; den Hartog, J. H. J.; Marcelis, A. T. M.; Reedijk, J. *J. Am. Chem. Soc.* **1984**, *106*, 3644−3647.
(31) Wong, H. C.; Shinozuka, K.; Natile, G.; Marzilli, L. G. *Inorg. Chim. Acta* **2000**, *297*, 36−46.
(32) Saad, J. S.; Scarcia, T.; Natile, G.; Marzilli, L. G., submitted.
(33) Sullivan, S. T.; Ciccarese, A.; Fanizzi, F. P.; Marzilli, L. G. *Inorg. Chem.* **2000**, *39*, 836−842.
(34) Sullivan, S. T.; Ciccarese, A.; Fanizzi, F. P.; Marzilli, L. G. *Inorg. Chem.* **2001**, *40*, 455−462.

Table 1. Atropisomer Percentages and H8 Chemical Shifts (ppm) of (**CCC**)Pt**G**$_2$ Complexes at 5 °C and Different pH Values

complex	pH	% ΛHT (ppm)	% ΔHT (ppm)	% HH (ppm)
(*S*,*R*,*R*,*S*)-**Me$_2$DAB**Pt(1-Me-5′-GMP)$_2$	3.6	69 (8.53)	6 (8.20)	25 (8.01, 8.94)
	7.6	54 (8.63)	6 (8.24)	40 (8.03, 9.15)
(*R*,*S*,*S*,*R*)-**Me$_2$DAB**Pt(1-Me-5′-GMP)$_2$	3.3	6 (8.25)	69 (8.82)	25 (8.10, 8.94)
	7.3	2 (8.43)	71 (9.12)	27 (8.20, 9.24)
(*S*,*R*,*R*,*S*)-**Bip**Pt(1-Me-5′-GMP)$_2$	3.3	62 (8.51)	9 (8.26)	29 (8.09, 8.94)
	7.3	48 (8.55)	8 (8.27)	44 (8.13, 9.10)
(*R*,*S*,*S*,*R*)-**Bip**Pt(1-Me-5′-GMP)$_2$	3.4	6 (8.24)	67 (8.74)	27 (8.11, 8.90)
	7.4	5 (8.41)	66 (8.90)	29 (8.19, 9.12)
(*S*,*R*,*R*,*S*)-**Me$_2$DAB**Pt(5′-GMP)$_2$[a]	3.2	82 (8.54)	6 (8.28)	12 (8.01, 8.95)
	7.1	96 (8.60)	1 (8.28)	3 (8.05, 9.19)
(*R*,*S*,*S*,*R*)-**Me$_2$DAB**Pt(5′-GMP)$_2$[a]	3.1	7 (8.27)	73 (8.73)	20 (8.09, 8.95)
	7.3	14 (8.37)	71 (8.88)	15 (8.14, 9.22)
(*S*,*R*,*R*,*S*)-**Bip**Pt(5′-GMP)$_2$[b]	3.0	83 (8.50)	6 (8.23)	11 (7.91, 9.01)
	7.0	95 (8.53)	2 (8.33)	3 (8.06, 9.16)
(*R*,*S*,*S*,*R*)-**Bip**Pt(5′-GMP)$_2$[b]	3.0	9 (8.24)	73 (8.62)	18 (8.07, 8.90)
	7.0	16 (8.37)	68 (8.73)	16 (8.16, 9.16)

[a] Reference 32. [b] Reference 15.

typical experiment, a selective presaturation pulse (30 dB) was applied for 2 s to the residual HOD resonance. The FID was accumulated for 64 transients in blocks containing 16K data points. Before Fourier transformation, the FIDs were baseline corrected for dc offset before an exponential multiplication apodization function with a 0.2 Hz line broadening was applied. NMR spectra were recorded at increments of ~0.3−0.5 pH unit. The percent of a conformer determined by integration is assumed to be accurate within 2%.

The 2D phase-sensitive NOESY spectra were performed at 5 °C with 64 scans per t_1 increment, a 512 × 2048 matrix, and a 500 ms mixing time. Each block of data was preceded by four dummy scans, and a spectral width of 6250 Hz was applied. A presaturation pulse of 1−2 s and a 10 ms delay were typically used for each acquisition. Data were processed using Felix 97.0 (MSI) on a Silicon Graphics INDY workstation. An exponential apodization function with a line broadening of 1 Hz in t_2 and zero-filling with 2K points for both dimensions were used before the Fourier transformation was applied.

CD samples of ~4×10^{-5} M 1-Me-5′-GMP were prepared by diluting aliquots from the NMR samples. Spectra were collected (λ = 200−400 nm) on a JASCO 600 spectropolarimeter at room temperature. Four scans recorded in succession were averaged to improve the signal/noise ratio.

pH Jump. This experiment was designed to determine the CD spectrum of conformers of retro models with very slow rates of atropisomerization.[28] First, the ^{1}H NMR and CD spectra of (*S*,*R*,*R*,*S*)-**Bip**Pt(1-Me-5′-GMP)$_2$ were recorded at pH ~ 3. The pH was then raised to ~7, and the ^{1}H NMR and CD spectra were acquired immediately. Spectra were then recorded at pH ~ 7 after 6 h and 2 days. Next, the pH was dropped to ~3, and the ^{1}H NMR and CD spectra were acquired immediately. Finally, these spectra were recorded at pH ~ 3 after 2 days. This experiment allowed us to deconvolute the CD spectra for the HH and HT conformers. The actual population of each form of (*S*,*R*,*R*,*S*)-**Bip**Pt(1-Me-5′-GMP)$_2$ was determined by integrating the H8 and H1′ NMR signals. For each wavelength, the CD spectra at a given pH are described by

$$Ax + By + Cz = Q$$
$$A'x + B'y + C'z = R$$
$$A''x + B''y + C''z = S$$

where Q, R, and S are the observed intensity values at times 0, 6 h, and 2 days, respectively, A, B, and C are the fractions of the HH, ΛHT, and ΔHT conformers, respectively, and x, y, and z are the deconvoluted intensity values of the HH, ΛHT, and ΔHT conformers, respectively. Because the distribution of the ΔHT conformer changed only slightly (1−2%), and because the ΛHT and ΔHT conformers have roughly opposite CD features, we set $z = -y$.

Molecular Modeling. MMD calculations were carried out on the 1-Me-5′-GMP complexes with all phosphate groups monoprotonated to mimic low pH conditions as described elsewhere.[35]

Results

The ^{1}H NMR H8 shifts of (**CCC**)Pt(1-Me-5′-GMP)$_2$ adducts have patterns very similar to those reported for the (**CCC**)Pt(5′-GMP)$_2$ adducts (Table 1).[15,27,32] A brief review of the reported interpretation of shifts, which relied on solid-state and solution structural results, is useful before we describe the (**CCC**)Pt(1-Me-5′-GMP)$_2$ results.

In the solid state, extensive structural data are available on the typical *cis*-Pt**A**$_2$**G**$_2$ complexes.[36−47] The HT forms observed cluster into two groups differing in the direction of the tilt (or cant);[5,42,44,46,47] i.e., the bases can have either a left-handed (L) or a right-handed (R) tilt, illustrated in Figure 4. The bases also can have a low or a high degree of canting.

(35) Yao, S.; Plastaras, J. P.; Marzilli, L. G. *Inorg. Chem.* **1994**, *33*, 6061−6077.
(36) Cramer, R. E.; Dahlstrom, P. L.; Seu, M. J. T.; Norton, T.; Kashiwagi, M. *Inorg. Chem.* **1980**, *19*, 148−154.
(37) Marzilli, L. G.; Chalilpoyil, P.; Chiang, C. C.; Kistenmacher, T. J. *J. Am. Chem. Soc.* **1980**, *102*, 2480−2482.
(38) Kistenmacher, T. J.; Chiang, C. C.; Chalilpoyil, P.; Marzilli, L. G. *J. Am. Chem. Soc.* **1979**, *101*, 1143−1148.
(39) Barnham, K. J.; Bauer, C. J.; Djuran, M. I.; Mazid, M. A.; Rau, T.; Sadler, P. J. *Inorg. Chem.* **1995**, *34*, 2826−2832.
(40) Lippert, B.; Raudaschl, G.; Lock, C. J. L.; Pilon, P. *Inorg. Chim. Acta* **1984**, *93*, 43−50.
(41) Schöllhorn, H.; Raudaschl-Sieber, G.; Müller, G.; Thewalt, U.; Lippert, B. *J. Am. Chem. Soc.* **1985**, *107*, 5932−5937.
(42) Grabner, S.; Plavec, J.; Bukovec, N.; Di Leo, D.; Cini, R.; Natile, G. *J. Chem. Soc., Dalton Trans.* **1998**, *9*, 1447−1451.
(43) Orbell, J. D.; Taylor, M. R.; Birch, S. L.; Lawton, S. E.; Vilkins, L. M.; Keefe, L. J. *Inorg. Chim. Acta* **1988**, *152*, 125−134.
(44) Cini, R.; Grabner, S.; Bukovec, N.; Cerasino, L.; Natile, G. *Eur. J. Inorg. Chem.* **2000**, *7*, 1601−1607.
(45) Sindellari, L.; Schöllhorn, H.; Thewalt, U.; Raudaschl-Sieber, G.; Lippert, B. *Inorg. Chim. Acta* **1990**, *168*, 27−32.
(46) Sinur, A.; Grabner, S. *Acta Crystallogr., Sect. C* **1995**, *51*, 1769−72.
(47) Kozelka, J.; Fouchet, M.-H.; Chottard, J.-C. *Eur. J. Biochem.* **1992**, *205*, 895−906.

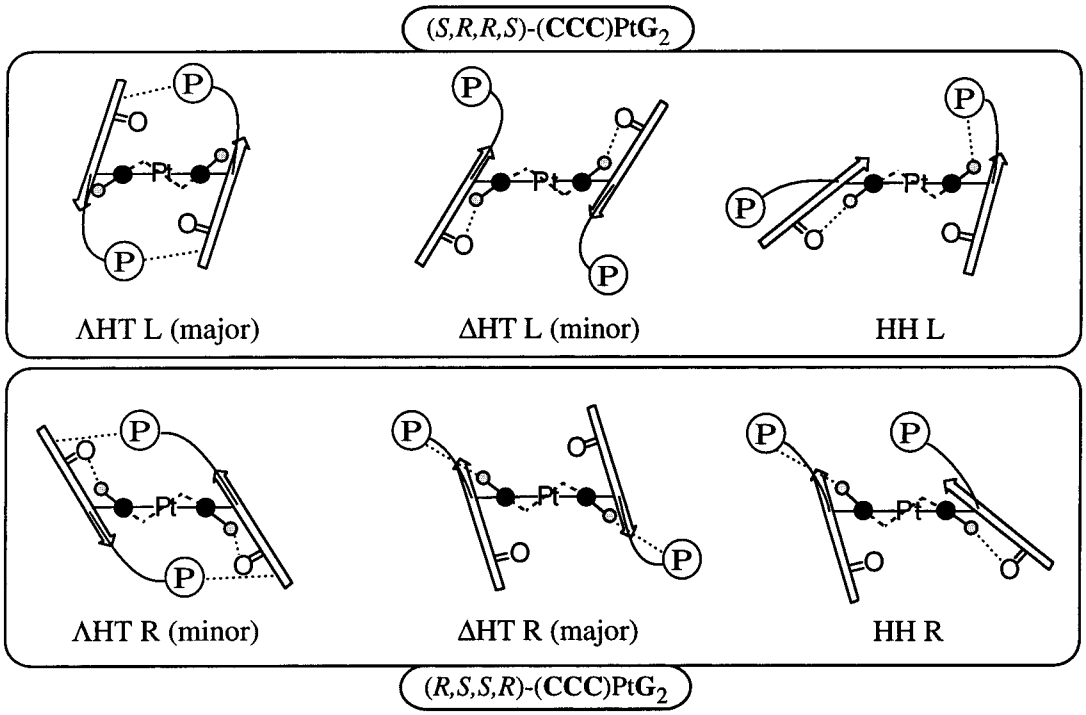

Figure 4. Sketches of the HT and HH rotamers of (*S*,*R*,*R*,*S*)- and (*R*,*S*,*S*,*R*)-(**CCC**)Pt**G**$_2$ with left-handed and right-handed cant, respectively, using arrows to represent N7-bound **G** bases as shown in Figure 1. The **Me$_2$DAB** and **Bip** ligands are shown more completely in Figure 3, but for clarity we show here only some components shared in common. (Nitrogen atoms are heavily shaded, while hydrogen atoms are lightly shaded.) Because base canting is now well supported by the data, we attempt to depict it fairly accurately. Sugar and phosphate groups are shown as curved lines and circled P's, respectively. The drawing indicates that the phosphate is directed toward the *cis*-**G** in the ΛHT form and toward the carrier ligand in the ΔHT form. However, because considerable flexibility exists in these groups, the position is not easily defined. All distances that potentially could lead to a hydrogen bond are indicated by a dotted line. However, the evidence provides support for SSC only in the ΛHT forms.

For dynamic *cis*-PtA$_2$**G**$_2$ models where **G** = nucleosides and nucleotides, the ΔHT forms were observed exclusively in the solid state;[36−39,48] all of the ΔHT forms had right-handed-canted bases. A high canting degree allowing **G** O6−NH hydrogen bonding has been found only when the **G** derivative is not a 5′-nucleotide or when the base is in an oligonucleotide;[40−42,44−46,49,50] in solid-state structures of 5′-nucleotide complexes, the direction of canting is unfavorable for **G** O6−NH H-bonding, which is absent or weak.[9,36,39,46,48] We now have extensive evidence *in solution* that bases in retro models cant and that the tilt direction and degree of tilt can be high or low, even for **G** = nucleosides and nucleotides, in some cases.[15,26,27,32−34] Also, we found that the **CCC** ligand chirality determines the cant direction;[15,27] the *R*,*S*,*S*,*R* chirality favors R canting, and the *S*,*R*,*R*,*S* chirality favors L canting.[15,27,32] This influence of the **CCC** ligand on canting has been found for all **G** derivatives and also for dinucleotides.[15−17,26,27,51]

For (**CCC**)Pt**G**$_2$ adducts,[15,24,26,27,32] the H8 signal of the major HT form is downfield from the H8 signal of the minor HT form. When the **CCC** ligand has the *S*,*R*,*R*,*S* configuration, the ΛHT conformer is the major form and the ΔHT conformer is the minor form. When the **CCC** ligand has the enantiomeric *R*,*S*,*S*,*R* configuration, the preferred HT conformer is reversed; the ΔHT conformer is the major form and the ΛHT conformer is the minor form. In the dominant HT form, **G** O6−(NH)**CCC** hydrogen bonding is not possible because **G** O6 is on the wrong side of the coordination plane from the ligand NH group (Figure 4). In the minor HT conformer, **G** O6 lies on the NH side of the carrier ligand, potentially allowing participation in hydrogen bonding (Figure 4). The 1-Me-5′-GMP complexes studied here fit this pattern.

The H8 shift is influenced by the positioning of the H8 atom with respect to the shielding cone of the *cis*-**G**. This position is a consequence of two factors: the direction and the degree of cant (tilt). The tilting of the two equivalent bases in the direction, moving each H8 toward the *cis*-**G**, will lead to greater H8 shielding and hence an upfield H8 signal relative to the average H8 signal. This direction of canting occurs for the minor HT forms (ΔHT L and ΛHT R) (Figure 4). The interaction of the **G** H8 with the *cis*-**G** has a small steric effect and is associated with a rather high degree of tilting in X-ray data.[49] For minor HT forms, the **CCC** ligand should not impede base tilting because the **G** O6 is closer to the small NH side of the carrier ligand (Figure 4). In contrast, the tilting of the base, moving its H8 away from the *cis*-**G**, will lead to less H8 shielding or maybe deshielding[47] and hence a more downfield H8 signal; this occurs for the major HT forms (ΛHT L and ΔHT R). This direction of tilt places the larger six-membered rings of the two *cis*-**G** bases closer together than in the minor HT forms

(48) Gellert, R. W.; Bau, R. *J. Am. Chem. Soc.* **1975**, *97*, 7379−7380.
(49) Orbell, J. D.; Wilkoski, K.; De Castro, B.; Marzilli, L. G.; Kistenmacher, T. J. *Inorg. Chem.* **1982**, *21*, 813−821.
(50) Admiraal, G.; van der Veer, J. L.; de Graaff, R. A. G.; den Hartog, J. H. J.; Reedijk, J. *J. Am. Chem. Soc.* **1987**, *109*, 592−594.
(51) Ano, S. O.; Intini, F. P.; Natile, G.; Marzilli, L. G. *J. Am. Chem. Soc.* **1998**, *120*, 12017−12022.

(Figure 4) and is associated with a lower degree of canting in X-ray data.[46]

The equivalent bases in each HT form have H8 signals at shifts intermediate to those of the nonequivalent bases of the (**CCC**)Pt**G**$_2$ HH form. The **G** base of the (**CCC**)Pt**G**$_2$ HH form with O6 closest to the NH has the H8 atom positioned toward the *cis*-**G** and has a relatively upfield H8 signal, and the base with O6 closest to the NCH_3 or NCH_2 group has a downfield H8 signal.[15,24,26,27,32] This latter base is less canted, and its H8 probably is further away from the other **G**. The H8 signal (labeled HH_u) of the more canted **G** is the most upfield of the four (**CCC**)Pt**G**$_2$ H8 signals because this H8 is closest to the shielding region of the *cis*-**G**. The H8 signal (labeled HH_d) of the less canted base has the most downfield shift; this H8 is farthest from the *cis*-**G** shielding region and may be in the deshielding region.

Shifts of the H1′ and N1−CH_3 ^{1}H NMR signals of the 1-Me-5′-GMP ligand also provide probes of the structural features. The H1′ signal, while less dispersed than the H8 signal, follows the same trend. The N1−CH_3 group is on the opposite end of the base (schematically, on the tail of the arrow) from H8 (head of the arrow) (Figure 2). Canting places either the N1−CH_3 group or the H8 of a given base close to the shielding cone of the *cis*-**G**. The N1−CH_3 signal follows the trend opposite that of the H8 signal. For clarity, the N1−CH_3 NMR signals are labeled as HH_c (canted HH base, H8 upfield, N1−CH_3 downfield) and HH_n (not so canted base, H8 downfield, N1−CH_3 upfield). An analogous interpretation of the consequence of this head/tail relationship on the ^{1}H NMR signals of protons on different rings of lopsided ligands has been offered for ruthenium(II) and rhenium(V) trimethylbenzimidazole complexes.[52−56] This explanation can also be applied to Ru(II) complexes with other ligands[57−59] and Pt−IMP adducts.[32]

Characterization of Complexes. (*S*,*R*,*R*,*S*)-Me$_2$DABPt-(1-Me-5′-GMP)$_2$. At 5 °C, the four H8 signals, assigned with the NOESY spectrum at pH ∼ 7, had pH-dependent shifts (Figure 5 and Table 1). When the pH was raised from ∼3 to ∼7, the HH_d and ΛHT H8 signals shifted downfield (Figure 5 and Table 1), while the HH_u and ΔHT H8 signals shifted very slightly downfield. The HH conformer increased in abundance significantly to 40% (Table 1), an unexpected result for a *cis*-PtA_2**G**$_2$ adduct, an adduct type that for decades has been thought to favor the HT conformation almost exclusively.[36−39,60,61] Because the N1 proton of 5′-GMP is replaced with a methyl group in 1-Me-5′-GMP, no further changes were observed, as expected after the phosphate groups were fully deprotonated (above pH 7.5, Supporting Information).

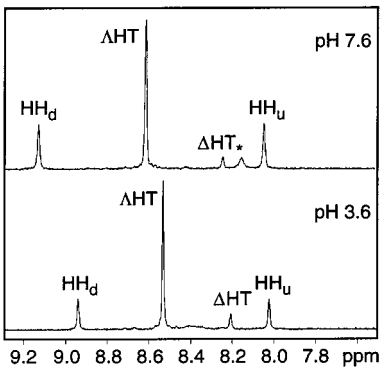

Figure 5. H8 ^{1}H NMR signals of (*S*,*R*,*R*,*S*)-**Me$_2$DAB**Pt(1-Me-5′-GMP)$_2$ at different pH values and 5 °C. Asterisk: H8 signal of free 1-Me-5′-GMP added at pH 7.6 to ensure complete reaction before the 2D NMR experiment.

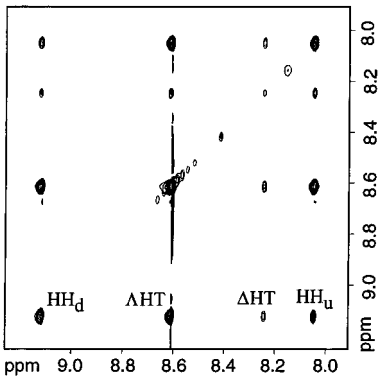

Figure 6. H8 region of the NOESY/EXSY NMR spectrum of (*S*,*R*,*R*,*S*)-**Me$_2$DAB**Pt(1-Me-5′-GMP)$_2$ at 5 °C and pH 7.6.

The H8−H8 exchange cross-peaks in the NOESY/EXSY spectrum at pH ∼ 7 (Figure 6) indicate interconversion among the three conformers on the NMR time scale, as observed for (*S*,*R*,*R*,*S*)-**Me$_2$DAB**Pt(5′-GMP)$_2$.[27] The H8−H1′ NOE cross-peak for the ΔHT form has undetectably low intensity (Figure 7). The ratio of the H8−H1′ NOE cross-peak volumes of the HH conformer (HH_u H1′/HH_d H1′) is 3.8. This is a novel spectral feature because the ratio should be close to unity if both 1-Me-5′-GMP ligands have similar structural features. The 3.8 volume ratio (Table 2) indicates that the time-averaged H8−H1′ distance in the 1-Me-5′-GMP with the canted base (HH_u signal) is smaller than in the 1-Me-5′-GMP with the uncanted base; thus, the residue with the canted base appears to have an unusually high amount of the *syn* conformation.[16]

(*S*,*R*,*R*,*S*)-BipPt(1-Me-5′-GMP)$_2$. Without the rapid atropisomer interconversion of the **Me$_2$DAB** analogue, the four H8 NMR signals of (*S*,*R*,*R*,*S*)-**Bip**Pt(1-Me-5′-GMP)$_2$ at 5 °C are sharp (Figure 8). When the pH was raised from ∼3 to ∼7, changes in the intensities and shifts of the H8 signals occurred. A large downfield shift for the HH_d signal (Figure 8 and Table 1), a lesser downfield shift for the ΛHT H8

(52) Marzilli, L. G.; Iwamoto, M.; Alessio, E.; Hansen, L.; Calligaris, M. *J. Am. Chem. Soc.* **1994**, *116*, 815−816.
(53) Alessio, E.; Calligaris, M.; Iwamoto, M.; Marzilli, L. G. *Inorg. Chem.* **1996**, *35*, 2538−2545.
(54) Alessio, E.; Hansen, L.; Iwamoto, M.; Marzilli, L. G. *J. Am. Chem. Soc.* **1996**, *118*, 7593−7600.
(55) Marzilli, L. G.; Marzilli, P. A.; Alessio, E. *Pure Appl. Chem.* **1998**, *70*, 961−968.
(56) Alessio, E.; Zangrando, E.; Iengo, E.; Macchi, M.; Marzilli, P. A.; Marzilli, L. G. *Inorg. Chem.* **2000**, *39*, 294−303.
(57) Iwamoto, M.; Alessio, E.; Marzilli, L. G. *Inorg. Chem.* **1996**, *35*, 2384−2389.
(58) Alessio, E.; Zangrando, E.; Roppa, R.; Marzilli, L. G. *Inorg. Chem.* **1998**, *37*, 2458−2463.
(59) Velders, A. H.; Hotze, A. C. G.; van Albada, G. A.; Haasnoot, J. G.; Reedijk, J. *Inorg. Chem.* **2000**, *39*, 4073−4080.
(60) Cramer, R.; Dahlstrom, P. *Inorg. Chem.* **1985**, *24*, 3420−3424.
(61) Isab, A.; Marzilli, L. G. *Inorg. Chem.* **1998**, *37*, 6558−6559.

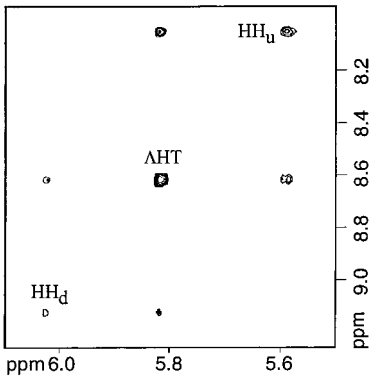

Figure 7. H8−H1′ region of the NOESY NMR spectrum of (*S,R,R,S*)-**Me$_2$DAB**Pt(1-Me-5′-GMP)$_2$ at 5 °C and pH 7.6. The ΔHT H8−H1′ cross-peak is very small and thus does not appear at this contour level. The unlabeled peaks are transfer NOE cross-peaks.[54]

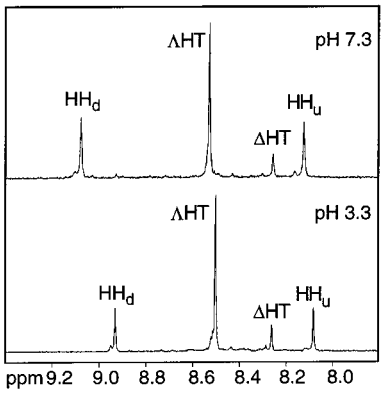

Figure 8. H8 ^{1}H NMR signals of (*S,R,R,S*)-**Bip**Pt(1-Me-5′-GMP)$_2$ at different pH values and 5 °C.

and HH$_u$ signals, and essentially no shift for the ΔHT H8 signal were observed. After equilibrium was reached at pH ∼ 7, the abundance of the HH conformer was 44%; *this marks the highest abundance of an HH conformer recorded for a cis-PtA$_2$**G**$_2$ adduct.*

The wide separation of the H1′ signals allows measurement of the $^3J_{H1'-H2'}$ constants (Table 3 and Supporting Information); a similar pattern of the H1′ signals was observed previously for other (**CCC**)Pt**G**$_2$ adducts.[27] For a given conformer, the H1′ shifts and couplings are very similar for **Me$_2$DAB**Pt(1-Me-5′-GMP)$_2$ and **Bip**Pt(1-Me-5′-GMP)$_2$ complexes at pH ∼ 3 and 7 (Table 3). The $^3J_{H1'-H2'}$ constants are useful for assessing qualitatively the S or N sugar pucker. We discuss the coupling data only for **Bip**Pt(1-Me-5′-GMP)$_2$ models because these complexes have sharper HH H1′ NMR signals. For a typical free **G** nucleotide, $^3J_{H1'-H2'}$ is ∼6.2−6.9 Hz;[62−65] the S/N ratio was calculated to be ∼77/23.[65] Upon platination, the $^3J_{H1'-H2'}$ values decrease to an average value of ∼4 Hz, indicating that the S/N sugar pucker equilibrium of nucleotides changes in the direction of N pucker, giving an S/N ratio of ∼60/40.[62,63,66−68] Interestingly, for (*S,R,R,S*)-**Bip**Pt(1-Me-5′-GMP)$_2$ at pH ∼ 3 and 7, the value of 6.5 Hz for $^3J_{H1'-H2'}$ of the 1-Me-5′-GMP residue with the canted base is correlated with a high amount of S pucker (S/N = ∼73/27); this value is 3.7 Hz for the H1′ signal of the 1-Me-5′-GMP residue with the uncanted base, indicating a higher percentage of N pucker (S/N = ∼41/59). For the ΛHT and ΔHT conformers, the relative S/N ratios were ∼55/45 and ∼66/34, respectively.

For (*S,R,R,S*)-**Bip**Pt(1-Me-5′-GMP)$_2$, the N1−CH$_3$ signals of the HH conformer were separated by ∼0.3 ppm. The N1−CH$_3$ signal of the ΛHT conformer was between these two signals, while the signal of the ΔHT conformer partially overlapped with the downfield signal of the HH conformer (HH$_c$) (Supporting Information). The chemical shift order of the N1−CH$_3$ signals of the three conformers is essentially the reverse of the H8 and H1′ chemical shift order.

In the NOESY spectrum at pH ∼ 7 used for assignment, the H8 signals at 8.13 and 9.10 ppm are connected by a strong NOE cross-peak (Supporting Information), a previously reported characteristic of the HH conformer. However, the HH$_u$ H1′ NOE cross-peak is 2.5 times stronger than the HH$_d$ H1′ peak (Table 2 and Supporting Information). This result indicates that the 1-Me-5′-GMP residue with the canted base exists in the *syn* conformation to a higher extent than the typical Pt−N7 bound **G** nucleotide.

(*R,S,S,R*)-Me$_2$DABPt(1-Me-5′-GMP)$_2$. The four H8 signals at 5 °C (Figure 9) were assigned by analogy to the 5′-GMP analogue.[24] At pH ∼ 3, the HH conformer of (*R,S,S,R*)-**Me$_2$DAB**Pt(1-Me-5′-GMP)$_2$ exists in higher abundance than the HH conformer of the respective 5′-GMP complex (Table 1). When the pH was raised to ∼7, almost no change occurred in the intensity of the H8 signals (Figure 9, Table 1); only a large downfield shift of the HH$_d$ and ΔHT H8 signals and a slight downfield shift for the HH$_u$ and ΛHT H8 signals were observed (Table 1).

(*R,S,S,R*)-BipPt(1-Me-5′-GMP)$_2$. At 5 °C, the four H8 signals of (*R,S,S,R*)-**Bip**Pt(1-Me-5′-GMP)$_2$ were assigned from the NOESY spectrum at pH ∼ 7 (Table 1 and Supporting Information). The intensity of the H8 signals of the (*R,S,S,R*)-**Bip**Pt(1-Me-5′-GMP)$_2$ conformers did not change over the pH range of ∼3−7. However, at pH ∼ 7 the H8 signals were significantly downfield (∼0.1−0.2 ppm), Table 1.

At pH ∼ 7, the NOE cross-peak between the H8 signals at 8.19 and 9.12 ppm (Supporting Information) is characteristic of the HH conformer. The HH$_u$ H1′ cross-peak is slightly stronger than the HH$_d$ H1′ cross-peak (Supporting Information and Table 2). This result indicates that the 1-Me-5′-GMP residue with the canted base favors the *syn* conformation more than the residue with the less canted base. However, the HH$_u$ H1′/HH$_d$ H1′ NOE cross-peak ratio is

(62) Marcelis, A. T. M.; van Kralingen, C. G.; Reedijk, J. *J. Inorg. Biochem.* **1980**, *13*, 213−222.
(63) Marcelis, A. T. M.; Erkelens, C.; Reedijk, J. *Inorg. Chim. Acta* **1984**, *91*, 129−135.
(64) Inagaki, K.; Dijt, F. J.; Lempers, E. L. M.; Reedijk, J. *Inorg. Chem.* **1988**, *27*, 382−387.
(65) Polak, M.; Plavec, J.; Trifonova, A.; Földesi, A.; Chattopadhyaya, J. *J. Chem. Soc., Perkin Trans. 1* **1999**, *19*, 2835−2843.
(66) Lempers, E. L. M.; Bloemink, M. J.; Reedijk, J. *Inorg. Chem.* **1991**, *30*, 201−206.
(67) Bloemink, M. J.; Dorenbos, J. P.; Heetebrij, R. J.; Keppler, B. K.; Reedijk, J.; Zahn, H. *Inorg. Chem.* **1994**, *33*, 1127−1132.
(68) Bloemink, M. J.; Heetebrij, R. J.; Ireland, J.; Deacon, G. B.; Reedijk, J. *J. Biol. Inorg. Chem.* **1996**, *1*, 278−283.

Table 2. Atropisomer H8−H1′ NOE Cross-Peak Volumes (Volume Unit) of (**CCC**)Pt(1-Me-5′-GMP)$_2$ Complexes at 5 °C

complex	pH	ΛHT	ΔHT	HH_u	HH_d	HH_u/HH_d
(*S*,*R*,*R*,*S*)-**Me$_2$DAB**Pt(1-Me-5′-GMP)$_2$	7.6	2.46	*a*	0.85	0.23	3.8
(*S*,*R*,*R*,*S*)-**Bip**Pt(1-Me-5′-GMP)$_2$	7.3	1.69	0.147	1.44	0.57	2.5
(*R*,*S*,*S*,*R*)-**Bip**Pt(1-Me-5′-GMP)$_2$	7.4	*a*	2.49	0.94	0.64	1.5

[a] Not determined because of their low intensity.

Table 3. H1′ Chemical Shifts and $^3J_{H1'-H2'}$ of (**CCC**)Pt(1-Me-5′-GMP)$_2$ Complexes at 5 °C and Different pH Values

		δ(H1′)/ppm ($^3J_{H1'-H2'}$/Hz)			
complex	pH	ΛHT	ΔHT	HH_u	HH_d
(*S*,*R*,*R*,*S*)-**Me$_2$DAB**Pt(1-Me-5′-GMP)$_2$	3.6	5.82 (4.8)	5.80 (*b*)	5.67 (*b*)	6.02 (*b*)
	7.6	5.82 (4.8)	5.76 (*b*)	5.60 (*b*)	6.03 (*b*)
(*R*,*S*,*S*,*R*)-**Me$_2$DAB**Pt(1-Me-5′-GMP)$_2$	3.3	5.98 (*a*)	5.98 (3.1)	5.81 (6.3)	6.07 (3.7)
	7.3	5.98 (*a*)	5.98 (3.2)	5.78 (6.4)	6.07 (3.7)
(*S*,*R*,*R*,*S*)-**Bip**Pt(1-Me-5′-GMP)$_2$	3.3	5.85 (4.9)	5.84 (*a*)	5.72 (6.5)	6.04 (3.6)
	7.1	5.81 (4.9)	5.77 (5.9)	5.66 (6.5)	6.03 (3.7)
(*R*,*S*,*S*,*R*)-**Bip**Pt(1-Me-5′-GMP)$_2$	3.4	5.97 (*a*)	5.94 (3.0)	5.79 (6.2)	6.03 (4.3)
	7.4	5.92 (*a*)	5.95 (3.1)	5.78 (6.3)	6.02 (4.2)

[a] Cannot be determined because of overlapped signals. [b] Coupling could not be measured because of the broadening.

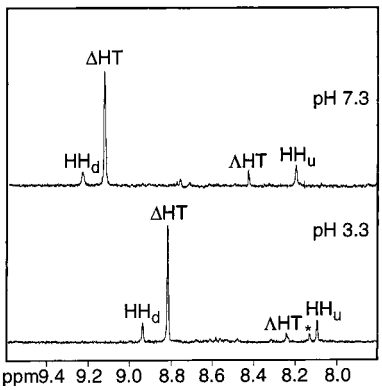

Figure 9. H8 ^{1}H NMR signals of (*R*,*S*,*S*,*R*)-**Me$_2$DAB**Pt(1-Me-5′-GMP)$_2$ at different pH values and 5 °C. The asterisk marks the free 1-Me-5′-GMP signal at pH 3.3, overlapped at pH 7.3.

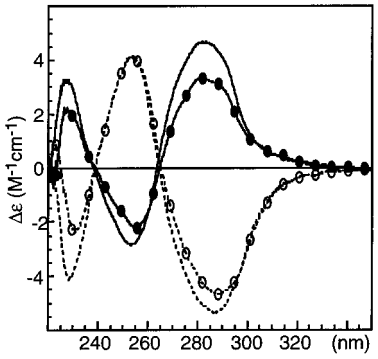

Figure 10. CD spectra of (*S*,*R*,*R*,*S*)-**Me$_2$DAB**Pt(1-Me-5′-GMP)$_2$ (solid) and (*R*,*S*,*S*,*R*)-**Me$_2$DAB**Pt(1-Me-5′-GMP)$_2$ (dashed) at pH 3.4. Open and closed circles are at pH 7.6.

lower for (*R*,*S*,*S*,*R*)-**Bip**Pt(1-Me-5′-GMP)$_2$ than for (*S*,*R*,*R*,*S*)-**Me$_2$DAB**Pt(1-Me-5′-GMP)$_2$ and (*S*,*R*,*R*,*S*)-**Bip**Pt(1-Me-5′-GMP)$_2$ complexes (Table 2). Thus, the *syn* conformation is more favorable in the latter compounds.

The HH conformer of (*R*,*S*,*S*,*R*)-**Bip**Pt(1-Me-5′-GMP)$_2$ exhibits a sugar conformation similar to that of (*S*,*R*,*R*,*S*)-**Bip**Pt(1-Me-5′-GMP)$_2$, as revealed by $^3J_{H1'-H2'}$ values (Table 3). However, the major HT conformer (ΔHT) of (*R*,*S*,*S*,*R*)-**Bip**Pt(1-Me-5′-GMP)$_2$ has a larger percentage of the N pucker (S/N = ∼33/67) than the major HT conformer (ΛHT) of (*S*,*R*,*R*,*S*)-**Bip**Pt(1-Me-5′-GMP)$_2$ (S/N = ∼55/44).

CD Spectroscopy. The CD spectrum of the (*S*,*R*,*R*,*S*)-(**CCC**)Pt**G**$_2$ adduct has features with signs opposite to those of the (*R*,*S*,*S*,*R*)-(**CCC**)Pt**G**$_2$ adduct; however, the intensities of the CD features are not exactly the opposite for the adducts with a given **G** because the intensity of the CD spectral features reflects the conformer distribution existing in the sample solution and because the major ΛHT and ΔHT conformers are in any case diastereomers, not enantiomers. Nevertheless, the major HT conformer of (**CCC**)Pt**G**$_2$ adducts dictates the general shape of the mixture's CD spectrum.[15,27] For example, the CD features of (*R*,*S*,*S*,*R*)-**Me$_2$DAB**Pt(1-Me-5′-GMP)$_2$ are more intense and opposite in sign to those of (*S*,*R*,*R*,*S*)-**Me$_2$DAB**Pt(1-Me-5′-GMP)$_2$ (Figure 10). This relationship is consistent with the ^{1}H NMR findings at pH ∼ 3 and 7 (Table 1) that the abundance of the dominant conformer (ΔHT) of (*R*,*S*,*S*,*R*)-**Me$_2$DAB**Pt(1-Me-5′-GMP)$_2$ is higher than that of the dominant conformer (ΛHT) of (*S*,*R*,*R*,*S*)-**Me$_2$DAB**Pt(1-Me-5′-GMP)$_2$. At pH ∼ 7, the intensity of the features of the CD spectrum of (*S*,*R*,*R*,*S*)-**Me$_2$DAB**Pt(1-Me-5′-GMP)$_2$ decreased by ∼30% from that at pH ∼ 3.

***(S,R,R,S)*-(CCC)Pt(1-Me-5′-GMP)$_2$ Adducts.** The CD spectrum of (*S*,*R*,*R*,*S*)-**Me$_2$DAB**Pt(1-Me-5′-GMP)$_2$ at pH ∼ 3 has positive features at 285 and 227 nm and a negative feature at 252 nm (Figure 10). The shape of this spectrum has the characteristics of a ΛHT conformer,[15,27] which is the major form of (*S*,*R*,*R*,*S*)-**Me$_2$DAB**Pt(1-Me-5′-GMP)$_2$. The CD spectrum of (*S*,*R*,*R*,*S*)-**Bip**Pt(1-Me-5′-GMP)$_2$ at pH ∼ 3 (Figure 11) is very similar to that of (*S*,*R*,*R*,*S*)-**Me$_2$DAB**Pt-(1-Me-5′-GMP)$_2$. The CD spectrum of (*S*,*R*,*R*,*S*)-**Bip**Pt(1-Me-5′-GMP)$_2$ has positive features at 288 and 228 nm and a negative feature at 254 nm.

***(R,S,S,R)*-(CCC)Pt(1-Me-5′-GMP)$_2$ Adducts.** For (*R*,*S*,-*S*,*R*)-**Me$_2$DAB**Pt(1-Me-5′-GMP)$_2$, the shape of the CD spectrum (negative features at 285 and 227 nm and a positive feature at 252 nm) (Figure 10) is characteristic of a ΔHT conformer.[15,27] When the pH was raised from ∼3 to ∼7 for (*R*,*S*,*S*,*R*)-**Me$_2$DAB**Pt(1-Me-5′-GMP)$_2$, the negative features

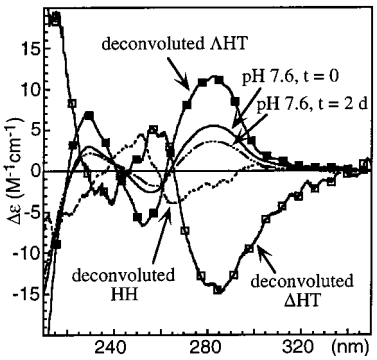

Figure 11. CD spectra of (*S*,*R*,*R*,*S*)-**Bip**Pt(1-Me-5′-GMP)$_2$ at pH 7.6. In the deconvoluted CD spectra, note the strong and weak CD features of the HT and HH conformers, respectively.

at 285 and 227 nm showed a *slight* decrease in intensity whereas the positive feature at 252 nm did not change. At pH ∼ 3, the CD spectrum of (*R*,*S*,*S*,*R*)-**Bip**Pt(1-Me-5′-GMP)$_2$ (not shown) was very similar to that of the respective **Me$_2$DAB** adduct (within ±3 nm). Two days after the pH was increased to ∼7, the CD features of (*R*,*S*,*S*,*R*)-**Bip**Pt(1-Me-5′-GMP)$_2$ had changed in the same manner as those of the respective **Me$_2$DAB** complex.

pH Jump. This experiment combines the results produced by two different spectroscopic methods (NMR and CD) to find and assess CD features of each form in a mixture of conformers of platinum complexes.[17] The deconvoluted CD spectrum at pH ∼ 7 of the HH, ΛHT, and ΔHT conformers of the (*S*,*R*,*R*,*S*)-**Bip**Pt(1-Me-5′-GMP)$_2$ complex was obtained by the pH jump method.

At pH ∼ 3, the abundances of the ΛHT, ΔHT, and HH conformers of (*S*,*R*,*R*,*S*)-**Bip**Pt(1-Me-5′-GMP)$_2$ were 62%, 9%, and 29%, respectively, as determined by H8 signals (Figure 8 and Table 1). The pH was raised to ∼7. An NMR spectrum was acquired immediately, but no change in abundance had occurred. After intervals of 6 h and 2 days at pH ∼ 7, the distribution had changed to 57%, 8%, and 35% and to 48%, 8%, and 44% for the ΛHT, ΔHT, and HH conformers, respectively. After that, the pH was lowered to ∼3 and the ^{1}H NMR spectrum was recorded immediately; the distribution was unchanged. After 2 days, the ^{1}H NMR spectrum was recorded again; the intensities of the H8 signals were the same as in the original spectrum at pH ∼ 3.

The CD spectra of the solutions just described were recorded; no change in intensity was observed when the pH was raised to ∼7 and the spectrum acquired immediately (Figure 11). The CD spectrum at pH ∼ 7 changed slowly over several hours as the population of the HH conformer increased. After 2 days, no further changes were observed, indicating that equilibrium had been reached.

Applying the equations given in the Experimental Section and combining both CD and NMR data and spectra at three different times (0, 6 h, and 2 days), we obtained the deconvoluted CD spectra of the ΛHT, ΔHT, and HH conformers. The HH conformer has weak deconvoluted CD features (negative feature at ∼265 nm, ∼−4 M^{-1} cm^{-1}; positive feature at ∼250 nm, ∼4 M^{-1} cm^{-1}). The deconvoluted CD spectrum of the ΛHT conformer shows strong features (positive features at ∼280 nm, ∼12 M^{-1} cm^{-1}, and at ∼230 nm, 7 M^{-1} cm^{-1}; negative feature at ∼250 nm, −7 M^{-1} cm^{-1}). The CD features of the ΔHT conformer are almost opposite to those of the ΛHT conformer (Figure 11).

Lowering the pH to ∼3 led to no changes in the CD spectrum recorded immediately, but the spectrum changed slowly with time. The CD spectrum recorded after the sample was left at pH ∼ 3 for 2 days had regained the original intensity.

Molecular Mechanics and Dynamics (MMD) Calculations. Calculations were performed for the three conformers of the four adducts studied here. The ΛHT conformer was computed to be the most stable conformer for (*S*,*R*,*R*,*S*)-(**CCC**)Pt(1-Me-5′-GMP)$_2$ adducts, and the ΔHT conformer has the lowest computed energy for the (*R*,*S*,*S*,*R*)-(**CCC**)-Pt(1-Me-5′-GMP)$_2$ models (Supporting Information). Calculated geometries were useful for designing experiments to assess conformations. However, because solvent was not included in the calculations, interesting computed structural features are mentioned briefly mainly in the Supporting Information.

Discussion

Influence on Structure of SSC and Identity of the CCC Ligand. At the beginning of the Results, we explained why the H8 chemical shift is very sensitive to structure. At pH values of ∼3 and ∼7, the H8 shifts of all 12 conformers for the four (*S*,*R*,*R*,*S*)- and (*R*,*S*,*S*,*R*)-(**CCC**)Pt(1-Me-5′-GMP)$_2$ complexes were very similar to those of the 12 respective analogous conformers of the four 5′-GMP complexes studied previously (Table 1).[15,32] These results indicate that the elimination of SSC by replacing N1H by a methyl group had almost no influence on the base canting because changes in canting would have been reflected clearly by differences in the H8 shifts of the conformers. The shifts of the H1′ signals lead to the same conclusion. In addition, as far as we can determine because the HH form is difficult to study for the 5′-GMP adducts, the sugar pucker indicated by H1′ coupling is similar for all 12 corresponding conformers of the four 1-Me-5′-GMP and 5′-GMP adducts. Thus, whatever role a 5′-PO$_4$−*cis*-**G** interaction plays in influencing the tilt degree of the bases and sugar pucker, the effects are the same whether there is a PO$_4$−N1H hydrogen bond or not. The major identifiable factor in controlling canting in these adducts is the **CCC** ligand. The increase in the N pucker on platination has been widely found.[20,62−64,69] At this time not enough is known to explain why sugars of some **G** derivatives are more prone than sugars of other **G** derivatives to adopt a high percentage of N pucker. However, for cross-linked adducts, including duplexes, the 5′-G residue seems to have high N pucker in the typical HH form.[5,6,70,71] We have now found the N pucker to occur for the 5′-G in various

(69) Talman, E. G.; Myers, D. P.; Reedijk, J. *Inorg. Chim. Acta* **1995**, *240*, 25−28.
(70) Mukundan, S., Jr.; Xu, Y.; Zon, G.; Marzilli, L. G. *J. Am. Chem. Soc.* **1991**, *113*, 3021−3027.
(71) Iwamoto, M.; Mukundan, S., Jr.; Marzilli, L. G. *J. Am. Chem. Soc.* **1994**, *116*, 6238−6244.

conformers of the cross-link.[5,14,16,17,51] MMD calculations on such cross-links always reveal this pucker for the low-energy form.[5,6,16,17,51] In contrast, MMD calculations on these simpler 1-Me-5′-GMP and 5′-GMP adducts do not provide insight into factors influencing the sugar pucker.

This is the first study using four **CCC** ligands in parallel experiments. It is important to note that, although the spectra and distributions are slightly different, each **Me$_2$DAB**Pt(1-Me-5′-GMP)$_2$ adduct behaves essentially the same as the corresponding **Bip**Pt(1-Me-5′-GMP)$_2$ adduct. As discussed below, the dynamic properties are very different. These data confirm the retro-model design focusing on destabilizing the transition state without altering the ground state. The results suggest that wagging of the base (i.e., fluctuation of the tilt angle about an average angle) either is not large or occurs to the same extent for adducts with the two ligands.

(*S*,*R*,*R*,*S*)-(CCC)Pt(1-Me-5′-GMP)$_2$ Adducts. A comparison of the conformer distributions for (*S*,*R*,*R*,*S*)-**Me$_2$DAB**Pt(1-Me-5′-GMP)$_2$ and (*S*,*R*,*R*,*S*)-**Bip**Pt(1-Me-5′-GMP)$_2$ to the distributions of the respective 5′-GMP complexes[15,32] is particularly informative (Table 1). In the previously studied (*S*,*R*,*R*,*S*)-(**CCC**)Pt(5′-GMP)$_2$ complexes (Table 1),[15,32] increasing the pH from ∼3 to ∼7 led to a very high dominance of the major ΛHT conformer. This increase is attributable to SSC (Figure 4). SSC (phosphate−N1H hydrogen bonding) should be stronger at pH ∼ 7 because the phosphate group is deprotonated, and in the ΛHT conformer the phosphate group is correctly positioned to interact with the N1H group (Figure 4). In contrast, a similar increase in pH from ∼3 to ∼7 caused quite different changes in the distribution of the (*S*,*R*,*R*,*S*)-(**CCC**)Pt(1-Me-5′-GMP)$_2$ complexes. Instead of increasing, the ΛHT conformer *decreased* in relative abundance, and it constitutes only ∼50% of the atropisomer distribution at pH ∼ 7 (Table 1). This finding provides strong confirmatory evidence for the important influence of SSC on the distribution of the 5′-GMP adducts.

For the 5′-GMP adducts, the increase in the ΛHT conformer from a pH value of ∼3 to a pH value of ∼7 came at the expense of both the HH and the ΔHT conformers (Table 1). The higher abundance of the HH conformer in a given *cis*-PtA$_2$**G**$_2$ series when **G** = 5′-GMP than for other **G** derivatives suggested a 5′-phosphate effect favoring the HH form. The nature of the effect was unknown, but instead of increasing on phosphate group deprotonation, the effect diminished as judged by the decreased abundance of the HH form at pH ∼ 7. This decrease in the HH form as the pH was raised from ∼3 to ∼7 was difficult to reconcile with the observation that the HH form is always most favored when **G** = 5′-GMP than when **G** is another derivative. For (*S*,*R*,*R*,*S*)-(**CCC**)Pt(1-Me-5′-GMP)$_2$ complexes, which lack the N1H necessary for stabilization of the ΛHT conformer, the HH form *increases* in abundance with an increase in pH (Table 1), consistent with the 5′-phosphate effect favoring the HH form. Similarly, instead of a decrease, the HH form of **Me$_2$ppz**Pt(1-Me-5′-GMP)$_2$, an adduct allowing neither SSC nor FSC, increased by 7% from 27% to 34% on phosphate deprotonation.[34] A larger increase (∼15%) was observed for (*S*,*R*,*R*,*S*)-(**CCC**)Pt(1-Me-5′-GMP)$_2$ HH forms. One of the two 1-Me-5′-GMP ligands in the HH form, the 1-Me-5′-GMP with the less canted base, has its phosphate group positioned so that a hydrogen bond interaction could occur with the *cis*-NH of the **CCC** ligand (Figure 4). Therefore, we cannot exclude the possibility that a component of the larger increase in the HH form of (*S*,*R*,*R*,*S*)-(**CCC**)Pt(1-Me-5′-GMP)$_2$ adducts than the **Me$_2$ppz**Pt(1-Me-5′-GMP)$_2$ adduct involves FSC. The new results (Table 1) confirm that the *decrease* in the HH form at pH ∼ 7 for the (*S*,*R*,*R*,*S*)-(**CCC**)Pt(5′-GMP)$_2$ complexes found in other studies[15,32,34] is due primarily to the dominance of the SSC effect at pH ∼ 7, favoring the more abundant ΛHT conformer.

The high abundance of the (*S*,*R*,*R*,*S*)-(**CCC**)Pt(1-Me-5′-GMP)$_2$ HH form allows us to identify some interesting features of this form. In particular, this left-handed HH form has a high amount of the *syn* conformation of the residue with the canted base. This conformation in plastic models suggests that the intraresidue PO$_4$−NH$_2$ distance might be short enough for hydrogen bonding. However, in our MMD calculations when we forced the phosphate group to be closer to the NH$_2$ group, the calculated energy was high (10 kcal/mol). Furthermore, the four ^{1}H NMR NH$_2$ signals in H$_2$O (pH 3.3) of (*S*,*R*,*R*,*S*)-**Bip**Pt(1-Me-5′-GMP)$_2$ were observed at 6.86 ppm (less canted HH), 7.00 ppm (canted HH), 6.92 ppm (ΛHT), and 7.05 ppm (ΔHT) (data not shown); these shifted only slightly at pH ∼ 7. Because the range of shifts of NH$_2$ signals is consistent with the cant of the bases and *cis*-**G** shielding, it is unlikely that the canted residue has a PO$_4$−NH$_2$ interaction, which would lead to the downfield shift of the HH NH$_2$ signal of the canted 1-Me-5′-GMP.

The *syn* conformation of the canted **G** and the *anti* conformation of the less canted **G** (*syn*,*anti* HH) could be caused by electrostatic repulsion between the deprotonated phosphate groups. In an *anti*,*anti* HH form, both phosphate groups are on the same side of the coordination plane. This may be electrostatically unfavorable, especially because one base is canted, bringing the two dianionic phosphate groups close together. However, a *syn*,*anti* HH form avoids this problem. The already high abundance of the (*S*,*R*,*R*,*S*)-(**CCC**)Pt(1-Me-5′-GMP)$_2$ HH form at low pH (where the monoprotonated phosphate groups offer less electrostatic repulsion) increases on phosphate deprotonation. For (**CCC**)-Pt(5′-GMP)$_2$ complexes, the low abundance of the HH conformer at pH values of ∼3 and ∼7 impeded any assessment of the *syn*,*anti* conformation of the 5′-GMP ligands.[15,32]

(*R*,*S*,*S*,*R*)-(CCC)Pt(1-Me-5′-GMP)$_2$ Adducts. The (*R*,*S*,*S*,*R*)-**CCC** ligand stabilizes the ΔHT conformer favored by right-handed canting. In our study of (*R*,*S*,*S*,*R*)-(**CCC**)-Pt(5′-GMP)$_2$ complexes, we showed that the abundance of the major ΔHT conformer decreases and that of the minor ΛHT conformer increases when the pH is increased from ∼3 to ∼7.[15,32] Because the minor ΛHT conformer is stabilized by SSC, the phosphate group deprotonation will further stabilize this form. For (*R*,*S*,*S*,*R*)-(**CCC**)Pt(1-Me-5′-GMP)$_2$ complexes, the absence of any significant change in the population distribution by increasing the pH from ∼3 to

~7 is due to the presence of the methyl group on the N1 position. No SSC is present to stabilize the ΛHT form.

For the previously studied (*R*,*S*,*S*,*R*)-(**CCC**)Pt(5′-GMP)$_2$ compounds, the major ΔHT conformer remains the favored and most abundant form at all pH values (Table 1).[15,32] It should be noted that if interaction of the phosphate group with the carrier ligand NH group (FSC) were important, the ΔHT conformer would have increased in abundance from pH ~ 3 to pH ~ 7. However, both this form and the HH form decrease when the phosphate group is deprotonated. These results indicate that SSC in the ΛHT form is more important than both FSC and the 5′-phosphate effect favoring the HH form.

As in the *S*,*R*,*R*,*S* analogue, the 1-Me-5′-GMP with the less canted base in the HH form of (*R*,*S*,*S*,*R*)-(**CCC**)Pt(1-Me-5′-GMP)$_2$ adducts has its phosphate group positioned so that a hydrogen-bonding interaction could occur with the *cis*-NH of the **CCC** ligand (Figure 4). The HH form of the (*R*,*S*,*S*,*R*)-(**CCC**)Pt(1-Me-5′-GMP)$_2$ complexes is right-handed, and thus the positioning is different from that in the *S*,*R*,*R*,*S* analogue (Figure 4). (*R*,*S*,*S*,*R*)-(**CCC**)Pt(1-Me-5′-GMP)$_2$ appears to contain a mix of the electrostatically unfavorable *anti*,*anti* HH form and the electrostatically favorable *syn*,*anti* HH form. The overall net electrostatic repulsion between the two dinegative phosphate groups may offset the FSC made favorable by deprotonation. Thus, phosphate group deprotonation does not stabilize the HH form or the ΛHT form (because **G** = 1-Me-5′-GMP), and the distribution is little changed between pH ~ 3 and pH ~ 7 (because FSC is weak or offset by phosphate−phosphate repulsion), Table 1.

Energy Barrier Concept Illustrated by the pH Jump Experiment. In **Me$_2$DAB** adducts, the *N*-methyl groups can rotate freely, and the chelate ring is rather flexible, thus allowing greater dynamic motion, as evidenced by EXSY cross-peaks connecting atropisomers in the 2D NOESY spectrum (Figure 6). The flexibility of the **Me$_2$DAB** ligand led us to design the more rigid **Bip** ligand, having two features: First, the chelate ring is part of the three-ring system that reduces the fluxional character. Second, the CH groups projecting toward the **G** coordination sites are unable to rotate away from the **G** bases during **G** rotation around the Pt−N7 bond. **Bip** and **Me$_2$DAB** have the same chirality characteristics (Figure 3) for a given isomer. The data show a great similarity in the NMR pattern and population distribution, but the great difference in the flexibility of the ligand leads to large differences in atropisomerization rates. Employing the **CCC** carrier ligands slowed the dynamic motion of the cisplatin−DNA adducts by a billionfold,[5,26] enabling us to elucidate aspects of the Pt−DNA adducts that are clouded by the dynamic motion problem. The atropisomer population distribution reflects ground-state stability, whereas the rate of interconversion of atropisomers reflects the activation energy barrier.

Briefly, we illustrate in Figure 12 the relationship between the ground-state free energies and activation barriers useful for understanding the pH jump experiment performed on the (*S*,*R*,*R*,*S*)-**Bip**Pt(1-Me-5′-GMP)$_2$ complex. The experiment

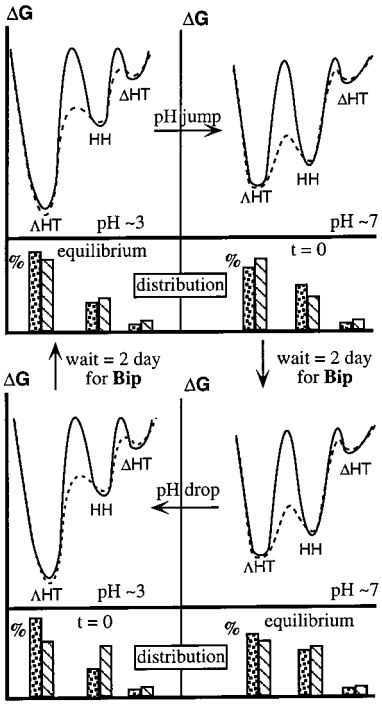

Figure 12. Illustration of the pH jump experiment. The free energy reaction profile is depicted by curved lines, and the conformer distribution (determined with ^{1}H NMR data) is represented by a bar graph. Solid curves and diagonal-line bars are used for (*S*,*R*,*R*,*S*)-**Bip**Pt(1-Me-5′-GMP)$_2$; dashed curves and dotted bars are used for (*S*,*R*,*R*,*S*)-**Me$_2$DAB**Pt(1-Me-5′-GMP)$_2$. Note that we do not know the relative vertical positions of the curves at pH ~ 3 vs pH ~ 7. The energy profiles depict the relative energies at the pH indicated. These energy profiles change immediately upon pH change. Upper left, pH ~ 3 and start of experiment, with both adducts at equilibrium. Distribution for (*S*,*R*,*R*,*S*)-**Bip**Pt(1-Me-5′-GMP)$_2$ (diagonal-line bars): upper right, pH ~ 7 immediately after the pH jump, a nonequilibrium distribution; lower right, pH ~ 7 after 2 days, equilibrium distribution; lower left, pH ~ 3 immediately after the pH drop, a nonequilibrium distribution; upper left, pH ~ 3 after 2 days, initial equilibrium distribution reestablished. Distribution for (*S*,*R*,*R*,*S*)-**Me$_2$DAB**Pt(1-Me-5′-GMP)$_2$ (dotted bars): after each pH adjustment, equilibration occurs immediately.

begins with aged solutions at pH ~ 3 containing the (*S*,*R*,*R*,*S*)-(**CCC**)Pt(1-Me-5′-GMP)$_2$ adducts with the three conformers at equilibrium. In Figure 12 (upper left), the percentage of each conformer is shown as a bar for each solution. The energy profile showing the ground-state energies (bottom of each well labeled, e.g., ΛHT) and activation barriers is shown for each adduct above the distribution. (Each "percentage" bar for each conformer is plotted under the relevant ground-state energy level; for a given conformer, the level is approximately the same for the two (*S*,*R*,*R*,*S*)-(**CCC**)Pt(1-Me-5′-GMP)$_2$ adducts.) The energy barriers between the conformers are shown to be higher for the **Bip** than the **Me$_2$DAB** cases to reflect the more dynamic nature of the latter conformers. When the pH is jumped from ~3 to ~7, the energy profile changes immediately with an increase in ground-state energy for the ΛHT form and a decrease in the HH form (Figure 12, upper right). The (*S*,*R*,*R*,*S*)-**Me$_2$DAB**Pt(1-Me-5′-GMP)$_2$ distribution responds immediately with a decrease in the ΛHT form and an increase in the HH form. In contrast, for (*S*,*R*,*R*,*S*)-**Bip**Pt-(1-Me-5′-GMP)$_2$, the distribution does not change immediately because the activation barriers are higher. CD spectra for (*S*,*R*,*R*,*S*)-**Bip**Pt(1-Me-5′-GMP)$_2$ can be recorded

for nonequilibrium situations; these spectra provide data for solving the deconvolution equations given in the Experimental Section. Eventually equilibrium is reached at pH ~ 7 (Figure 12, lower right). The HH conformer at pH ~ 7 now has an abundance comparable to that of the ΛHT conformer. Then the pH can be dropped to create another nonequilibrium situation, but now at pH ~ 3 (Figure 12, lower left).

Deconvolution of the CD Spectra. By applying the deconvolution formula for (*S*,*R*,*R*,*S*)-**Bip**Pt(1-Me-5′-GMP)$_2$, we obtained for the first time the deconvoluted CD spectrum of an HH conformer for a *cis*-type PtA_2**G**$_2$ adduct. In our previous studies of *cis*-PtA_2**G**$_2$, the CD features of the dominant HT conformer determined the overall CD spectrum, which was mainly shaped liked the signal of the dominant form.[15,27−29,31,33,34] We concluded that the shape is determined by the Δ or Λ chirality of the HT rotamer.[15,27−29,31,33,34] This interpretation conflicts with a previous suggestion that the shape is dictated by the handedness (R or L) of the HT conformer.[72,73] Deconvolution of the CD spectrum of the (*S*,*R*,*R*,*S*)-**Bip**Pt(1-Me-5′-GMP)$_2$ mixture confirms our interpretation. The HH conformer has weak CD features (negative at ~265 and positive at ~250 nm, Figure 11). In contrast, the deconvoluted CD signal of the major ΛHT conformer is much stronger (positive features at ~280 and ~230 nm and negative feature at ~250 nm, Figure 11). We also found recently that the deconvoluted CD signal of the HH conformer in a cross-linked adduct has weak features, while the CD features of the deconvoluted HT conformer are much stronger.[14,17] Thus, the results that HH forms have weak CD features and HT forms have strong features probably represent a general trend.

Conclusions. In contrast to the normal situation for simple cisplatin cross-link models, the system we have discovered has a rather stable HH form. Previous data from retro models indicated that a 5′-phosphate group favored both the ΛHT conformer and (to a lesser extent) the HH form. Although the reason that the HH form was favored was not known, our work suggested that the ΛHT conformer was favored by **G** phosphate−*cis*-**G** N1H hydrogen bonding, SSC. We eliminated this factor by using 1-Me-5′-GMP adducts. This strategy produced an unusually abundant (40−44%) HH left-handed conformer of (*S*,*R*,*R*,*S*)-(**CCC**)Pt(1-Me-5′-GMP)$_2$ complexes at pH ~ 7; this result clearly confirms the proposed role of SSC stabilization of the ΛHT conformer as a key element in influencing conformer distribution. Further support for this interpretation comes from the results in this study on (*R*,*S*,*S*,*R*)-(**CCC**)Pt(1-Me-5′-GMP)$_2$ adducts and from the study of **Me$_2$ppz**Pt(1-Me-5′-GMP)$_2$, in which a relatively abundant HH conformer was also observed at pH ~ 7.[34]

The clarity of the data afforded by an abundant HH form of a *cis*-PtA_2**G**$_2$ species provides several useful insights. First, the results suggest that the CD features of the HH form of a *cis*-PtA_2**G**$_2$ conformer are related to those of the HH form of the d(GpG) analogue.[14,22] Second, a 5′-phosphate effect favors the HH form for both 1-Me-5′-GMP and 5′-GMP adducts. Third, in the (*S*,*R*,*R*,*S*)-(**CCC**)Pt(1-Me-5′-GMP)$_2$ HH forms, the canted **G** adopts a *syn* conformation, making the repulsion at pH ~ 7 less severe. In the absence of SSC, the ΛHT form is not stabilized at pH ~ 7, so an unusually abundant HH form results from the 5′-phosphate effect. For **Me$_2$ppz**Pt(1-Me-5′-GMP)$_2$, the bases are not canted and both **G** ligands are *anti*.[34] The phosphate−phosphate repulsion is less severe at pH ~ 7 than for the (*R*,*S*,*S*,*R*)-(**CCC**)Pt(1-Me-5′-GMP)$_2$ HH form, in which one **G** is canted. The observed order of the abundance of the HH form is as follows: (*S*,*R*,*R*,*S*)-(**CCC**)Pt(1-Me-5′-GMP)$_2$ > (**Me$_2$ppz**)-Pt(1-Me-5′-GMP)$_2$ > (*R*,*S*,*S*,*R*)-(**CCC**)Pt(1-Me-5′-GMP)$_2$. This is also the order expected for increasing phosphate−phosphate repulsion.

Finally, the striking observation that FSC (phosphate to carrier ligand NH hydrogen bonding) need not be invoked to explain the stability of the ΔHT form for 5′-GMP complexes requires comment. In the solid state, numerous examples of ΔHT complexes of 5′-GMP and several related 5′-phosphate derivatives have been found not only for Pt with various carrier ligands, but also even for other metals.[36−47,74−77] The nucleotides in the structures have very similar relationships, with the purine bases having the same relative positions and the phosphate group always hydrogen-bonded to the *cis* ligand in a similar manner. This contrast between the prevalence of FSC in the solid and its relative unimportance in solution supports the premise of our retro-model studies that the structures in the solid state of dynamic nucleotide complexes may be very different from the solution structure.

Acknowledgment. This work was supported by NIH Grant GM 29222 (to L.G.M.), NATO Grant CRG 950376 (to L.G.M. and G.N.), MURST (contribution 40%), CNR, and EC (COST Chemistry Project D8/0012/97) (to G.N.).

Supporting Information Available: MMD methods and results, chemical shifts of N1−CH_3 groups of conformers of the (**CCC**)-Pt(1-Me-5′-GMP)$_2$ complexes, population distribution vs pH of the HT and HH atropisomers of (*S*,*R*,*R*,*S*)-**Me$_2$DAB**Pt(1-Me-5′-GMP)$_2$, 1D and 2D NMR spectra of (*S*,*R*,*R*,*S*)-**Bip**Pt(1-Me-5′-GMP)$_2$, 2D NMR spectra for (*R*,*S*,*S*,*R*)-**Bip**Pt(1-Me-5′-GMP)$_2$, and stereoviews of the minimum HH energy models of (*S*,*R*,*R*,*S*)- and (*R*,*S*,*S*,*R*)-(**CCC**)Pt(1-Me-5′-GMP)$_2$ from MMD calculations. This material is available free of charge via the Internet at http://pubs.acs.org.

IC010758Z

(72) Gullotti, M.; Pacchioni, G.; Pasini, A.; Ugo, R. *Inorg. Chem.* **1982**, *21*, 2006−2014.
(73) Pasini, A.; De Giacomo, L. *Inorg. Chim. Acta* **1996**, *248*, 225−230.
(74) Miller, S. K.; van der Veer, D. G.; Marzilli, L. G. *J. Am. Chem. Soc.* **1985**, *107*, 1048−1055.
(75) Begum, N. S.; Poojary, M. D.; Manohar, H. *J. Chem. Soc., Dalton Trans.* **1988**, *5*, 1303−1307.
(76) Mangani, S.; Orioli, P. *J. Chem. Soc., Chem. Commun.* **1985**, *12*, 780−781.
(77) Poojary, M. D.; Hattikudur, M. *J. Chem. Soc., Chem. Commun.* **1982**, *10*, 533−534.